Journal of Power Sources 229 (2013) 36–41

Contents lists available at SciVerse ScienceDirect

Journal of Power Sources

journal homepage: www.elsevier.com/locate/jpowsour

Phosphoric acid-imbibed three-dimensional polyacrylamide/poly(vinyl alcohol) hydrogel as a new class of high-temperature proton exchange membrane

Qunwei Tang [a], Kevin Huang [a,*], Guoqing Qian [b], Brian C. Benicewicz [b]

[a] Department of Mechanical Engineering, University of South Carolina, Columbia 29201, United States
[b] Department of Chemistry and Biochemistry, University of South Carolina, Columbia 29208, United States

HIGHLIGHTS

- PAM/PVA semi-IPN hydrogel membranes were employed to fabricate HTPEMFCs.
- The anhydrous proton conductivity reached 0.0525 S cm^{-1} at 183 °C.
- The unique absorption and retention of hydrogel membranes make them candidates in HTPEMs.

GRAPHICAL ABSTRACT

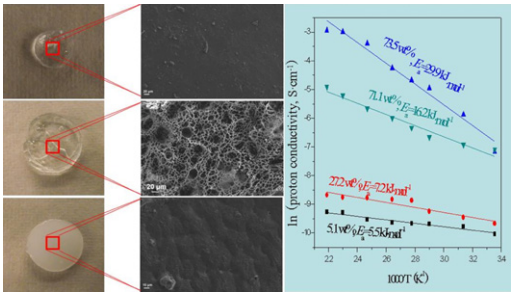

ARTICLE INFO

Article history:
Received 11 October 2012
Received in revised form
20 November 2012
Accepted 30 November 2012
Available online 10 December 2012

Keywords:
High-temperature proton exchange membrane
Fuel cells
Hydrogel
Polyacrylamide
Interpenetrating polymer network

ABSTRACT

This paper reports the first study that investigates H_3PO_4-imbibed polyacrylamide/poly(vinyl alcohol) (PAM/PVA) semi-interpenetrating polymer network (semi-IPN) hydrogel as a high-temperature proton exchange membrane (PEM). The extraordinary ability of the PAM/PVA hydrogel to absorb a large quantity of aqueous solution is fully utilized to achieve a high H_3PO_4 loading, resulting in high proton conductivity membranes. The anhydrous proton conductivity of a PAM/PVA semi-IPN hydrogel loaded with 73.5 wt% H_3PO_4 reaches 0.0525 S cm^{-1} at 183 °C in dry air. A fuel cell using the thick-film PAM/PVA hydrogel exhibits a peak power density of 0.225 W cm^{-2} at 183 °C with pure O_2 and H_2 as the oxidant and fuel, respectively. The synthesized membrane also shows excellent acid retention under mechanical load and high humidity, a valued characteristic for high-temperature PEMs. These performance-ensuring properties paired with a low-cost synthesis approach demonstrate the new membrane to be a viable candidate as a high-temperature PEM.

1. Introduction

Fuel cells offer efficient and clean energy conversion from chemical fuels into electricity. Of all the types of fuel cells, the proton exchange membrane fuel cell (PEMFC) stands out to be the most developed one with broadly gained scientific/engineering knowledge base for potentially widespread commercial use in stationary and transportation power generation sectors [1–3]. However, today's state-of-the-art Nafion-based PEMFC technology will need to further improve on its durability and economy in order to become a competitive commercial product. The extremely low tolerances to CO and H_2S [4], degradation of cathode performance associated with agglomerations of Pt-electrocatalysts nanoparticles and corrosion of carbon support [5,6], complicated and expensive water management [7], and high cost of electrocatalysts [8], are among key issues hindering the commercialization of PEMFC

* Corresponding author.
E-mail address: huang46@cec.sc.edu (K. Huang).

0378-7753/$ – see front matter © 2012 Elsevier B.V. All rights reserved.
http://dx.doi.org/10.1016/j.jpowsour.2012.11.134

technology. One solution to address many of these issues is to have PEMFC operated at a temperature higher than 100 °C. The benefits gained from an elevated operating temperature encompass enhanced tolerance to fuel impurities such as CO and H_2S, elimination of water management, improved electrode kinetics, increased likelihood of using non-precious metals as catalysts, higher conductivity and smaller heat exchangers or radiators [7,9,10]. To take advantage of high-temperature PEMFCs, the state-of-the-art Nafion-based PEMs must be replaced with alternative membrane materials of chemical stability. Anhydrous blends of basic polymers such as polyethers [11], polyamines [12], polyalcohols [13], polyamides [14] or poly(benzimidazole) (PBI) [15] with acids such as H_3PO_4 have been investigated previously as potential candidates. The polymer in these composite membranes serves as the support and immobilizer of the prime proton conducting phase H_3PO_4 [16], not necessarily as an intrinsic proton conductor. H_3PO_4-imbibed PBI membrane is a representative of this kind of composite proton conductor, in which the proton transfer is proposed to occur along pathways established by protons attached to benzimidazole rings surrounded by $H_2PO_4^-$ counterions [17]. By employing polyphosphoric acid as both solvent and polycondensation reagent, Benicewicz and co-workers have demonstrated that the PBI membrane can achieve high-performance and durability necessary for commercial high-temperature PEMFCs [18–20].

In the search for new classes of high-temperature PEMs, we have recently investigated the pertinent properties of crosslinked polyacrylamide (PAM) imbibed with H_3PO_4. Early work in this area was mainly focused on using either commercial PAM mixed with aqueous H_3PO_4 solution [14] or acrylamide monomer blended with an initiator to copolymerize with aqueous H_3PO_4 solution, for application in electrochromic windows [21–24]. The proton conductivity of thus formed composite membranes evaluated under hydrated state was in the order of 10^{-2} S cm^{-1} at ambient temperature [21–23] and in the order of 10^{-3} S cm^{-1} under anhydrous state at 100 °C [24]. Since the formed polymer had linear structure or non-crosslinked, it is more susceptible to water attack (partially soluble in water), limited H_3PO_4 loading (or attachment), non-uniform H_3PO_4 distribution, and poor thermal/chemical and mechanical stabilities.

Here we report for the first time the synthesis and characterization of a new class high-temperature proton conductor consisting of NMBA (*N*,*N*′-(methylene)bisacrylamide)-crosslinked 3D framework PAM imbibed with anhydrous H_3PO_4. Since the formed PAM membrane is a highly hydrophilic hydrogel, it allows H_3PO_4 to be easily incorporate into the 3D framework from its aqueous solution due to its large absorption capacity. The dried anhydrous H_3PO_4-imbibed PAM membrane has an excellent ability to retain H_3PO_4 and thermal/chemical stability at 100–200 °C. Poly(vinyl alcohol) (PVA) is also added to increase mechanical strength and film-forming capability of the resultant membrane by forming a semi-interpenetrating polymer network (semi-IPN). More importantly, high proton conductivity is warranted by the high H_3PO_4 loading benefited from the extraordinary "absorption" capability of hydrogel materials, the properties of which have been widely utilized in the areas of tissue engineering [25], artificial muscles [26], contact lens [27], drug delivery [28], sensors [29], and dye reclamation [30].

2. Experimental section

2.1. Synthesis of PAM/PVA semi-IPN composites

The PAM/PVA semi-IPN composites were synthesized according to a simple two-steps method described in our previous reports [31,32]. In detail, a mixture solution **1** consisting of acrylamide monomer (7.5 g, 99+%, electrophoresis grade) and crosslinker *N*,*N*′-(methylene)bisacrylamide (0.002 g, NMBA, 96%) was made by agitating in DI-water (10 mL) in a water-bath at 90 °C. Under the vigorous stirring, ammonium persulfate (APS, 98%) (0.015 g) was added to the above mixture. With the proceeding of polymerization, the viscosity increased gradually. When the viscosity of the PAM pre-polymers reached around 140 mPa s^{-1}, another homogeneous solution **2** consisting of PVA (hydrolyzed, M_w = 16,000, 1.2 g) and NMBA (0.002 g) was added. To continue the polymerization, another 0.015 g of APS was added into the above reagent solution until the viscosity of the system reached around 180 mPa s^{-1}. Finally, the reagent was poured into a Petri dish and cooled to room temperature with the formation of an elastic transparent gel. The PAM/PVA membranes were then molded into φ 3 cm die. After rinsing with DI-water, the membranes were dried under vacuum at 50 °C for 24 h.

2.2. Preparation of H_3PO_4-imbibed PAM/PVA semi-IPN membranes

The dried PAM/PVA semi-IPN membranes were immersed in H_3PO_4 aqueous solution with concentration varying from 0.1 to 10 M in a sealed bottle at room temperature for 3 days to reach absorption equilibrium. The resultant product was then filtered and dried under vacuum at 60 °C for 2 days to drive off all water as much as possible and obtain the final H_3PO_4-imbibed PAM/PVA hydrogel membranes. The actual H_3PO_4 loading (wt%) was determined by titration with 0.1 M sodium hydroxide as the neutralizer. Every sample was first mixed in 20 mL of previously boiled (to remove carbon dioxide) DI-water and allowed to stir for at least 30 min, followed by titrating using a Metrohm 716 DMS Titrino titrator. The first equivalence point was used to determine the volume of sodium hydroxide necessary for neutralization.

2.3. Electrochemical characterizations

The proton conductivity of the H_3PO_4-imbibed PAM/PVA membranes in either hydrous or anhydrous state were characterized with ac-impedance spectroscopy using a Zahner IM6 Electrochemical Workstation (ZAHNER-Electrik Gmbh & Co., Kronach, Germany) in a frequency range of 0.04 Hz–1 MHz and an ac amplitude of 10 mV in temperature range of 25–183 °C. Double coated PELCO Tabs™ carbon conductive tapes (TED PELLA, INC, 90% of polymer acrylic adhesive and 10% of carbon black) with a thickness of 0.1 mm were used as the electrodes. The ohmic resistance associated with the membrane was determined from the high frequency intersection of the spectrum with the Z′ axis, from which the proton conductivity can be calculated based on dimensional information.

2.4. Evaluation of H_3PO_4 retention

To evaluate the H_3PO_4 retention ability of H_3PO_4-imbibed PAM/PVA membrane, the membranes with 73.5 wt% H_3PO_4 loading were placed in an oven at 80 °C and mechanical pressure of 2.1×10^4 Pa with or without 100% RH air. Thus treated samples were then titrated to determine the loss of H_3PO_4.

2.5. Membrane electrode assembly (MEA) and fuel cell tests

The gas diffusion electrodes (GDE, acquired from BASF Fuel Cell, Inc., formerly E-Tek, Inc.) with a platinum loading of 1.0 mg cm^{-2}, were used for this study. The MEA with an active area of 10 cm^2 was fabricated by hot-pressing a H_3PO_4-imbibed PAM/PVA membrane between the two Kapton framed electrodes. The MEA was then

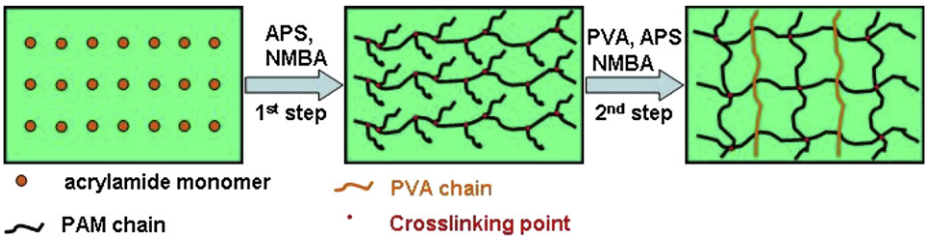

Fig. 1. Schematic of a "two-step" synthesis of the PAM/PVA semi-IPN membrane.

assembled into a single cell fuel cell testing rig. The gas flow fields were made from graphite plates with single serpentine gas channels. Stainless steel end plates with attached heaters were used to clamp the graphite flow plates. A commercial fuel cell testing station (Fuel Cell Technology, Inc.) was used for fuel cell testing, while H_2 and air or pure oxygen were fed to the anode and cathode without any humidification, respectively. The instrument was controlled by home-programmed LabView Software (National Instruments, Austin, TX).

2.6. Other characterizations

The morphologies of the hydrous and anhydrous H_3PO_4-imbibed PAM/PVA membranes were captured with a Zeiss Ultra Plus field emission scanning electron microscopy (FESEM). To observe the internal 3D microstructure of the membrane after water was removed, a swollen H_3PO_4-imbibed PAM/PVA membrane was first cut into ultrathin films, followed by loading into a chamber under freezing temperature and high vacuum to remove water. Fourier transform infrared spectrometry (FTIR) spectra were recorded on a PerkinElmer spectrum 100 FTIR spectrometer in an ATR mode.

3. Results and discussion

3.1. Structural analysis

The crosslinking of 3D framework hydrogel of hydrophilic PAM in the presence of film-forming facilitator PVA is schematically illustrated in Fig. 1 [31,32]. A mechanism for the polymerization process of the membrane is proposed in the Supporting information, along with more details on the synthesis of H_3PO_4-imbibed PAM/PVA semi-IPN membranes.

The physical appearance of the as-synthesized PAM/PVA membrane is shown in Fig. 2a, the microstructure of which was revealed by SEM to be fully dense with no open pores. After the membrane was imbibed in concentrated H_3PO_4 aqueous solution, its volume was appreciably enlarged, Fig. 2c, by the accommodation of water and H_3PO_4 molecules into the 3D hydrogel framework. To reveal the interconnected porous microstructure of the H_3PO_4-imbibed swollen PAM/PVA semi-IPN hydrogel membrane, the sample was freeze-dried. The microstructure shown in Fig. 2c indicates that the resultant PAM/PVA hydrogel membrane is indeed a well-interconnected, interpenetrating network capable of holding a large amount of H_3PO_4 in the microporous structure. Interestingly, the membrane imbibed with anhydrous H_3PO_4 becomes fully dense after being dried at 60 °C, Fig. 2b. At this stage, the imbibed H_3PO_4 molecules appear completely caged inside the PAM/PVA semi-IPN matrix and either form hydrogen bonds with the electronegative atoms such as O and N in O–H, C–N, C=O and NH_2 groups abundant in the framework of PAM/PVA semi-IPN, or establish its own proton conduction pathways via its P=O···H–O hydrogen bonds. The protons can then migrate along these hydrogen bonds throughout the membrane by successive proton transfer and reorientation steps [33] schematically shown in Fig. 2d. It is noteworthy to mention that the loading of H_3PO_4 aqueous solution by PAM/PVA semi-IPN membrane is driven by osmotic pressure gradient across the membrane [34], in which the H_3PO_4 imbibing occurs at a molecular scale. Upon driving off water molecules during the dehydration step, the 3D PAM/PVA semi-IPN molecular chains shrink, leaving the imbibed H_3PO_4 caged inside the 3D framework. The nature of H_3PO_4 being caged inside the 3D framework of the membrane gives rise to an excellent acid retention ability. In contrast, the permeation of H_3PO_4 into a pre-existing porous structure is mainly due to the capillary force of the nano-/micro-pores [9,35,36]. Thus incorporated H_3PO_4 molecules can easily escape from their host porous structure under conditions different from which H_3PO_4 molecules were originally imbibed.

The formation of hydrogen bonds in the PAM/PVS membranes was confirmed by the comparison of FTIR spectra between pure PAM/PVA and H_3PO_4-imbibed PAM/PVA membranes shown in Fig. 3. The absorption bands at 1681 (C=O stretching), 1456 (C–N stretching), 1224 (NH_2 wagging), and 992 (O–H deformation) cm^{-1} of the pure PAM/PVA were clearly shifted to lower wave numbers, *i.e.*, 1652, 1426, 1202, and 948 cm^{-1}, respectively, for the 63.0 wt% H_3PO_4-imbibed PAM/PVA membrane. This shift is a sign of the formation and concentration of O–H···O=C and O–H···N–C

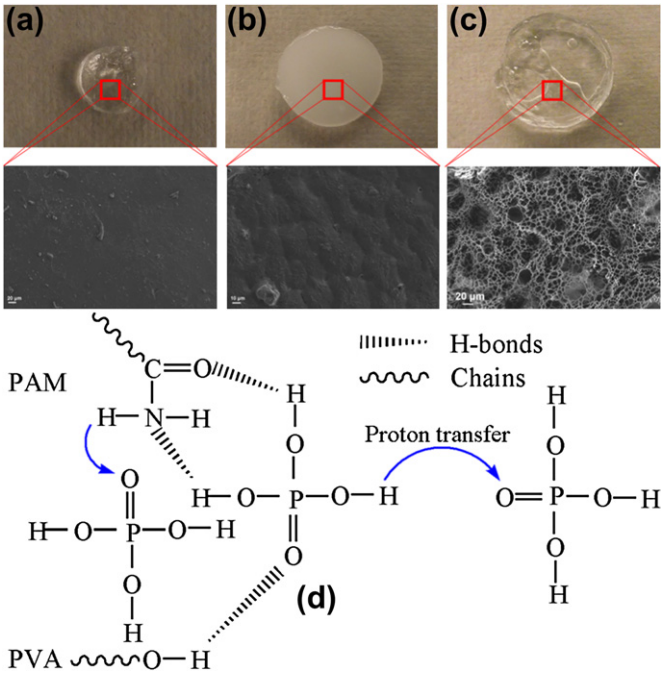

Fig. 2. Cross-sectional microstructures of (a) as-synthesized, (b) anhydrous H_3PO_4-imbibed PAM/PVA membrane (H_3PO_4 loading: 73.5 wt%), (c) as-swollen by H_3PO_4 aqueous solution, and (d) proposed proton transfer mechanism in H_3PO_4-imbibed PAM/PVA semi-IPN membrane under anhydrous conditions.

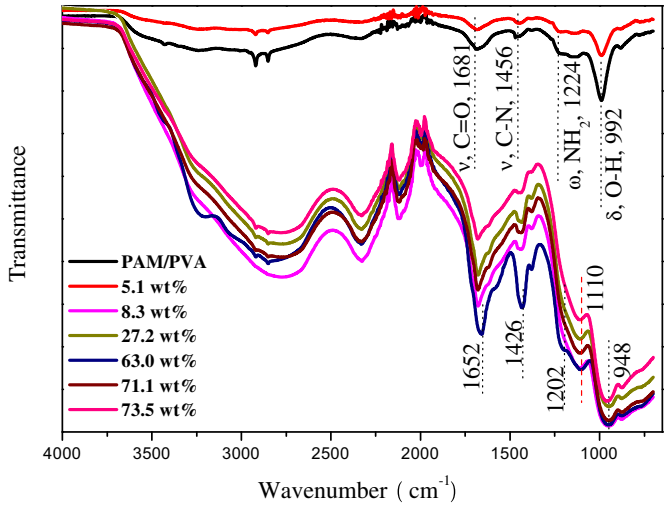

Fig. 3. FTIR spectra of pure PAM/PVA semi-IPN and H_3PO_4-imbibed PAM/PVA membranes.

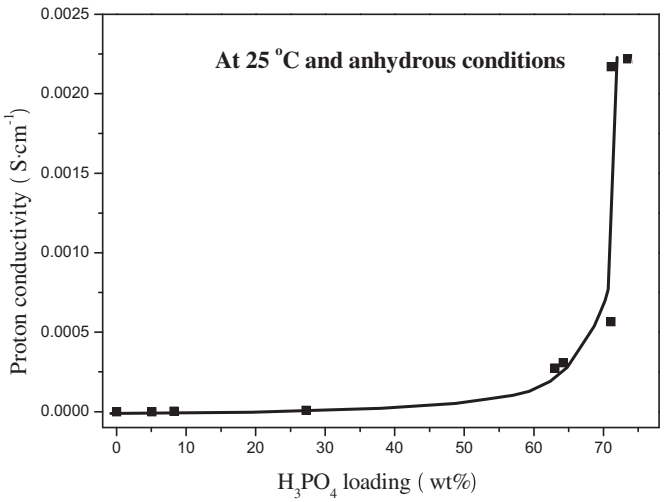

Fig. 5. Room temperature proton conductivity of anhydrous H_3PO_4-imbibed PAM/PVA membranes as a function of H_3PO_4 loading.

hydrogen bonds [14,37]. The membrane with the maximum H_3PO_4 loading of 73.5 wt% showed the greatest shift, indicating the highest concentration of hydrogen bonds formed. The presence of $H_2PO_4^-$ moieties at 1110 cm^{-1} further implies that the transport of protons may occur via Grotthuss mechanism, involving exchange of protons between Bronsted-type acid (H_3PO_4) and Bronsted-type base ($H_2PO_4^-$).

3.2. Proton conductivity

The proton conductivity of the membrane measured under dry air from 25 to 183 °C followed an Arrhenius relationship reasonably well as shown in Fig. 4a. It is interesting to note that the activation energy, E_a, systematically increases with the H_3PO_4 loading, which is opposite to that of H_3PO_4-doped PBI membranes [38], but similar to that of linear PAM/H_3PO_4 membranes [14]. Only at higher H_3PO_4 loading was E_a closer to that of pure H_3PO_4 (E_a = 23.05 kJ mol^{-1}). The much lower E_a at lower H_3PO_4 loading seems to suggest a different proton conduction mechanism from that of pure H_3PO_4. We hypothesize that at low H_3PO_4 loading, protons in H_3PO_4 form hydrogen bonds in low concentration with the functional group hosts C═O, C–N, NH_2 or O–H in PAM/PVA semi-IPN. These hydrogen bonds serve as the pathways for proton transfer as illustrated in Fig. 2d. The exceptionally low E_a seems to suggest that such a proton transfer is a facile process, but the low conductivity is mainly the result of low concentration of protons or hydrogen bonds formed between H_3PO_4 and PAM/PVA semi-IPN matrix. As the H_3PO_4 loading increases, H_3PO_4 itself eventually forms a percolated network to transfer protons, as shown in Fig. 4b [14]. This is also the reason why E_a at higher H_3PO_4 loading is closer to that of pure H_3PO_4 [16].

An important feature of conductive composite materials is that their overall conductivity is strongly influenced by the volumetric fractions of constituents in the materials [39,40]. The H_3PO_4-imbibed PAM/PVA membrane is no exception. The ambient temperature conductivity of this membrane is shown in Fig. 5 as a function of the loading of H_3PO_4. The proton conductivity is clearly seen to vary with H_3PO_4 loading in a range up to four orders of magnitude. At ambient temperature, the measured conductivity of a pure anhydrous PAM/PVA is 2.06×10^{-8} S cm^{-1}, compared to 2.22×10^{-3} S cm^{-1} of that with 73.5 wt% H_3PO_4 loading. An abrupt increase in conductivity is observed at around 60 wt% H_3PO_4, suggesting it the threshold for the formation of percolating proton pathways. The conductivity response of the membrane can be described by traditional percolation theory:

$$\sigma = C|f - f_c|^{\beta} \quad (1)$$

where σ is the proton conductivity, f is the weight percent of H_3PO_4 in the membrane, f_c is the percolation threshold where the

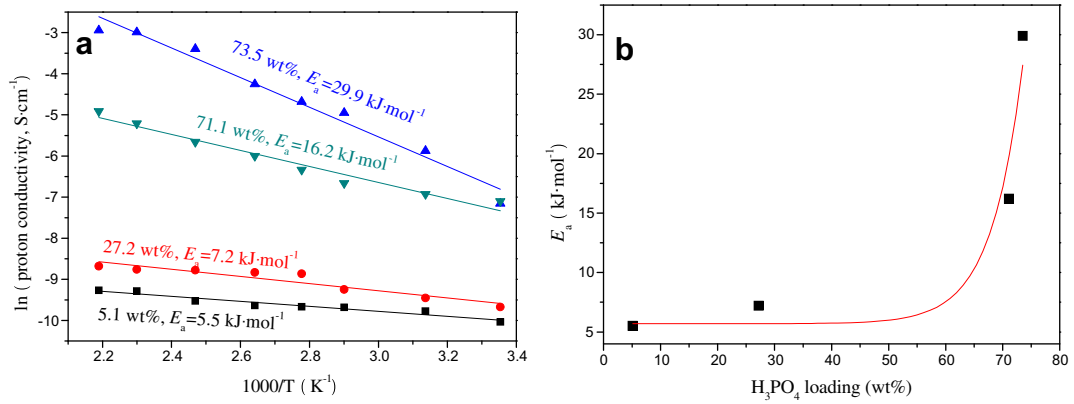

Fig. 4. Arrhenius plots for proton conductivity of H_3PO_4-imbibed PAM/PVA semi-IPN membranes measured under anhydrous conditions.

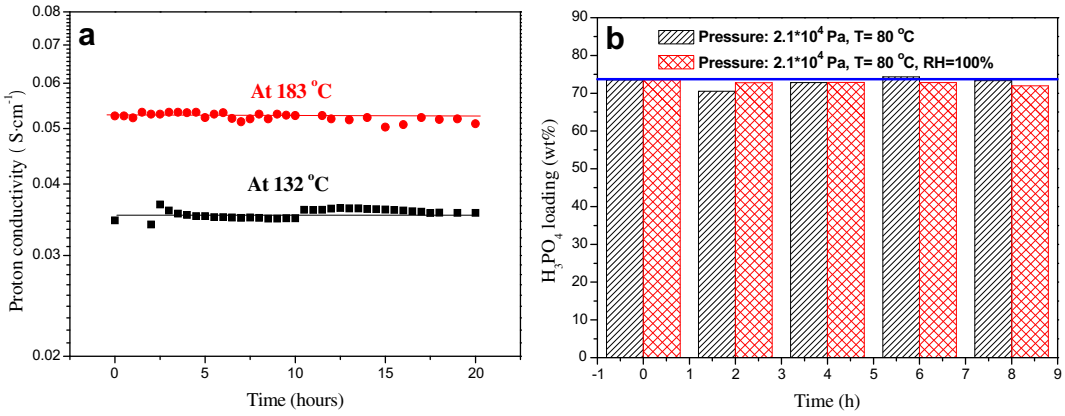

Fig. 6. (a) Stability of proton conductivity of H_3PO_4-imbibed PAM/PVA membranes (H_3PO_4 loading: 73.5 wt%), measured under anhydrous condition. (b) H_3PO_4 retention ability under a load of 2.1×10^4 Pa and in air with RH = 100% at 80 °C.

transition takes place, C is a constant, and β is the critical exponent (an index of system dimensionality, theoretically 1.3 and 1.94 for ideal 2D and 3D systems, respectively [39]). The H_3PO_4 fraction at which an insulator–conductor transition is observed refers to as the percolation threshold. In order to determine the percolation threshold, we have fitted the experimental data with Eq. (1) and the resultant fitting is drawn as the solid line in Fig. 5. The best fit yields $f_c = 58.4$ wt% and $\beta = 2$, which is very close to 1.94 for a 3D percolated network of randomly distributed particles. This makes sense in that these membranes behave like a 3D framework as the membrane thickness is considerably greater than the size of H_3PO_4 molecules. However, the same phenomenon is not observed in H_3PO_4-doped PBI membranes [41]. The percolation threshold value for conductivity in Fig. 5 is almost the same to that for shown in Fig. 4b, further supporting the formation of percolated H_3PO_4-networks.

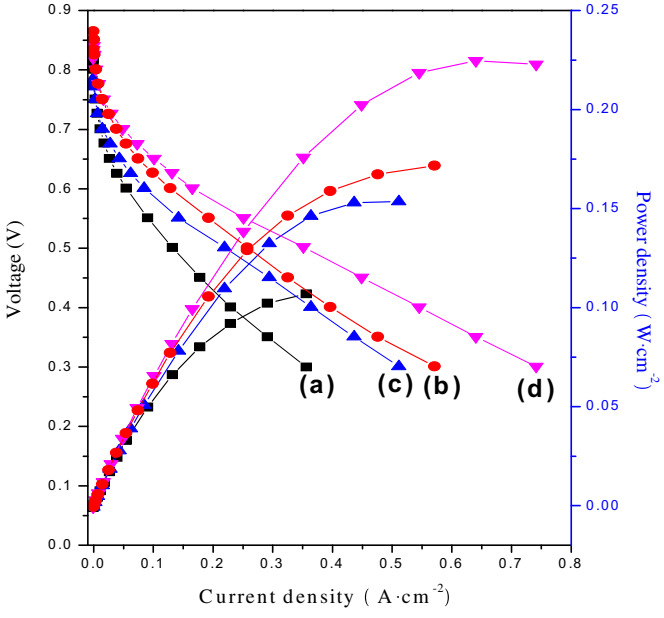

Fig. 7. V–I and P–I characteristics of H_3PO_4-imbibed PAM/PVA membranes with 73.5 wt% H_3PO_4 loading at 183 and 132 °C under anhydrous conditions. (a) H_2/air, 132 °C, (b) H_2/O_2, 132 °C, (c) H_2/air, 183 °C, and (d) H_2/O_2, 183 °C. Gas flow rates: H_2 1.2 stoich, air 2 stoich, O_2 2 stoich.

3.3. Stability

The conductivity stability of the H_3PO_4-imbibed PAM/PVA membranes (73.5 wt% H_3PO_4 loading) measured under anhydrous conditions is shown in Fig. 6a for two different temperatures. No sign of degradation can be detected during the short 20-h measurement. The measured anhydrous proton conductivity was 0.0525 S cm^{-1} at 183 °C, the highest among chemically similar but structurally linear systems. Interestingly, the H_3PO_4 contents determined under a mechanical pressure of 2.1×10^4 Pa and air with 100% RH at 80 °C remain relatively unchanged in Fig. 6b, suggesting that the membrane possesses a good H_3PO_4 retention ability. This unique ability may be attributed to the "cage" effect from the 3D framework formed during the dehydration process.

3.4. Fuel cell performance

A H_3PO_4-imbibed PAM/PVA membrane with a thickness of 500 μm was eventually assembled into a fuel cell for performance evaluation. Detailed description of fuel cell assembly can be found in the Experimental section. The V–I and P–I characteristics measured at 132 and 183 °C with dry H_2 as the fuel and dry air or pure oxygen as the oxidant are shown in Fig. 7. A maximum power density of 225 mW cm^{-2} @ 0.64 A cm^{-2} was achieved at 183 °C with pure oxygen as the oxidant. While the demonstrated performance is lower compared to the hydrated Nafion [42] and H_3PO_4-doped PBI [43], the overall performance is satisfactory and comparable to other proposed PEMFCs [7,44–46], considering the fact that both membrane and electrode were not optimized. The cell ohmic resistance was approximately 30 mΩ at 183 °C, which is close to the calculated membrane resistance of ~32 mΩ using the conductivity shown in Fig. 4a. The sharp decrease in voltage at low current density signals a high activation polarization of the electrode limiting the overall cell performance.

4. Conclusions

In summary, a new class of H_3PO_4-imbibed crosslinked 3D framework PAM/PVA semi-IPN composite polymers have been synthesized as high-temperature PEMs by a simple, low-cost, two-step approach. The synthesized membranes have an excellent H_3PO_4 retention ability and are thermally stable and mechanically strong. The protons transfer via the Grotthuss mechanism, migrating across hydrogen bonds present in H_3PO_4 as well as those formed between H^+ in H_3PO_4 and the functional groups C═O, C–N,

NH_2 and O–H in PAM/PVA. The H_3PO_4 is effectively caged inside the 3D framework after dehydration, mitigating the loss of H_3PO_4. A high and stable anhydrous proton conductivity of 0.0525 S cm^{-1} is obtained at 183 °C. A fuel cell using a thick membrane as a PEM showed a peak power density of 0.225 W cm^{-2} with O_2 and H_2 as the oxidant and fuel, respectively. These attributes demonstrate the PAM/PVA to be a viable high-temperature PEM. More importantly, the idea to use 3D framework hydrogel materials as a matrix to imbibe intrinsic proton conductors can be applied to other systems such as nonionic hydrogels with high salt-resistance and high absorbency to enhance H_3PO_4 loading and therefore proton conductivity. The thermal and mechanical performances and water absorbency can also be improved by combining clays with polyelectrolytes, such as starch-graft-polyacrylamide/kaolinite [47] and poly(acrylate-co-acrylamide)/vermiculite systems [48], which constitutes our future development.

Acknowledgments

We would like to acknowledge University of South Carolina for providing seed funding to this project. The authors also thank Prof. Chuanbing Tang and Dr. Kejian Yao for helping the measurement of FTIR spectra and processing samples for SEM observation.

Appendix A. Supplementary data

Supplementary data related to this article can be found at http://dx.doi.org/10.1016/j.jpowsour.2012.11.134.

References

[1] R. Bashyam, P. Zelenay, Nature 443 (2006) 63–66.
[2] S. Moghaddam, E. Pengwang, Y.B. Jiang, A.R. Garcia, D.J. Burnett, C.J. Brinker, R.I. Masel, M.A. Shannon, Nature Nanotechnology 5 (2009) 230–236.
[3] O. Diat, G. Gebel, Nature Materials 7 (2008) 13–14.
[4] V. Mazumder, Y.M. Lee, S.H. Sun, Advanced Functional Materials 20 (2010) 1224–1231.
[5] M. Miu, I. Kleps, M. Danila, T. Ignat, M. Simion, A. Bragaru, A. Dinescu, Fuel Cells 10 (2010) 259–269.
[6] A. Stein, Z.Y. Wang, M.A. Fierke, Advanced Materials 21 (2009) 265–293.
[7] S.Y. Lee, A. Ogawa, M. Kanno, H. Nakamoto, T. Yasuda, M. Watanabe, Journal of the American Chemical Society 132 (2010) 9764–9773.
[8] M. Lefevre, E. Proietti, F. Jaouen, J.P. Dodelet, Science 324 (2009) 71–74.
[9] J. Weber, K.D. Kreuer, J. Maier, A. Thomas, Advanced Materials 20 (2008) 2595–2598.
[10] S.Y. Kim, S. Kim, M.J. Park, Nature Communications 1 (2010) 88.
[11] J. Kerres, F. Schonberger, A. Chromik, M. Hein, Th. Haring, Q.F. Li, J.O. Jensen, P. Noye, N.J. Bjerrum, Fuel Cells (2008) 175–187.
[12] K. Tsuruhara, M. Rikukawa, K. Sanui, N. Ogata, Y. Nagasaki, M. Kato, Electrochimica Acta 45 (2000) 1385–1389.
[13] P.N. Gupta, K.P. Singh, Solid State Ionics 86–88 (1996) 319–323.
[14] D. Rodriguez, C. Jegat, O. Trinquet, J. Grondin, J.C. Lassègues, Solid State Ionics 61 (1993) 195–202.
[15] J. Hu, H. Zhang, Y. Zhai, G. Liu, J. Hu, B. Yi, Electrochimica Acta 52 (2006) 394–401.
[16] Y.L. Ma, J.S. Wainright, M.H. Litt, R.F. Savinell, Journal of the Electrochemical Society 151 (2004) A8–A16.
[17] Q.F. Li, J.O. Jensen, R.F. Savinell, N.J. Bjerrum, Progress in Polymer Science 34 (2009) 449–477.
[18] L. Xiao, H. Zhang, T. Jana, E. Scanlon, R. Chen, E.W. Choe, L.S. Ramanathan, S. Yu, B.C. Benicewicz, Fuel Cells 5 (2005) 287–295.
[19] L. Xiao, H. Zhang, E. Scanlon, L.S. Ramanathan, E.W. Choe, D. Rogers, T. Apple, B.C. Benicewicz, Chemistry of Materials 17 (2005) 5328–5333.
[20] J.A. Mader, B.C. Benicewicz, Macromolecules 43 (2010) 6706–6715.
[21] W. Wieczorek, Z. Florjanczyk, J.R. Stevens, Electrochimica Acta 40 (1995) 2327–2330.
[22] J. Przyluski, Z. Poltarzewski, W. Wieczorek, Polymer 39 (1997) 4343–4347.
[23] E. Wieczorek, J.R. Stevens, Polymer 38 (1997) 2057–2065.
[24] D. Raducha, W. Wieczorek, Z. Florjanczyk, J.R. Stevens, The Journal of Physical Chemistry 100 (1996) 20126–20133.
[25] D. Mawad, E. Steward, D.L. Officer, T. Romeo, P. Wagner, K. Wagner, Wallace, Advanced Functional Materials 22 (2012) 2692–2699.
[26] E.A. Moschou, S.F. Peteu, L.G. Bachas, M.J. Madou, S. Daunert, Chemistry of Materials 16 (2004) 2499–2502.
[27] C.C. Peng, M.T. Burke, A. Chauhan, Langmuir 28 (2012) 1478–1487.
[28] G.T. Franzesi, B. Ni, Y.B. Ling, A. Khademhosseini, Journal of the American Chemical Society 128 (2006) 15064–15065.
[29] L.A. DeLouise, P.M. Fauchet, B.L. Miller, A.A. Pentland, Advanced Materials 17 (2005) 2199–2203.
[30] Q.W. Tang, J.H. Wu, J.M. Lin, Q.H. Li, S.J. Fan, Journal of Materials Science 43 (2008) 5884–5890.
[31] Q.W. Tang, X.M. Sun, Q.H. Li, J.H. Wu, J.M. Lin, Journal of Colloid and Interface Science 339 (2009) 45–52.
[32] Q.W. Tang, X.M. Sun, Q.H. Li, J.H. Wu, J.M. Lin, Colloids and Surfaces A 346 (2009) 91–98.
[33] K.D. Kreuer, Solid State Ionics 136–137 (2000) 149–160.
[34] P.J. Flory, Principles of Polymer Chemistry, Cornel University Press, New York, 1953.
[35] D. Mecerreyes, H. Grande, O. Miguel, E. Ochoteco, R. Marcilla, I. Cantero, Chemistry of Materials 16 (2004) 604–607.
[36] Y.G. Jin, S.Z. Qiao, Z.P. Xu, J.C.D. da Costa, G.Q. Lu, The Journal of Physical Chemistry C 113 (2009) 3157–3163.
[37] R. Bouchet, E. Siebert, Solid State Ionics 118 (1999) 287–299.
[38] J.A. Asensio, S. Borrós, P. Gómez-Romero, Journal of the Electrochemical Society 151 (2004) A304–A310.
[39] W. Wang, K. Fernando, Y. Lin, M.J. Mexiani, L.M. Veca, L. Cao, P. Zhang, M.M. Kimani, Y.P. Sun, Journal of the American Chemical Society 130 (2008) 1415–1419.
[40] A.V. Kyrylyuk, M.C. Hermant, T. Schilling, B. Klumperman, C.E. Koning, P. Schoot, Nature Nanotechnology 6 (2011) 364–369.
[41] Q. Li, R. He, J.O. Jensen, N.J. Bjerrum, Fuel Cells 4 (2004) 147–159.
[42] V.D. Noto, M. Bettiol, F. Bassetto, N. Boaretto, E. Negro, S. Lavina, F. Bertasi, International Journal of Hydrogen Energy 37 (2012) 6169–6181.
[43] S. Yu, H. Zhang, L. Xiao, E.W. Choe, B.C. Benicewicz, Fuel Cells 4 (2009) 318–324.
[44] J. Zeng, S.P. Jiang, The Journal of Physical Chemistry C 115 (2011) 11854–11863.
[45] M. Georgezi, V. Deimede, N. Gourdoupi, N. Triantafyllopoulos, S. Neophytides, J.K. Kallitsis, Macromolecules 41 (2008) 9051–9056.
[46] K. Xu, H. Oh, M.A. Hickner, Q. Wang, Macromolecules 44 (2011) 4605–4609.
[47] J.H. Wu, Y.L. Wei, J.M. Lin, S.B. Lin, Polymer 44 (2003) 6513–6520.
[48] Q.W. Tang, J.M. Lin, J.H. Wu, Y. Xu, C. Zhang, Journal of Applied Polymer Science 104 (2007) 735–739.